Oxid Met (2014) 81:631–644
DOI 10.1007/s11085-014-9471-x

ORIGINAL PAPER

Hot Corrosion Behavior of a Ni_3Al-Based IC21 Alloy in a Molten Salt Environment

Wenyue Zhao · Yuzhuo Liu · Shusuo Li · Shengkai Gong

Received: 25 October 2013 / Revised: 3 January 2014 / Published online: 1 February 2014

Abstract Ni_3Al-based alloys have become important candidates for hot components in turbine engines, owing to their low densities and outstanding mechanical properties in service environments. The hot corrosion behavior of a Ni_3Al-based IC21 alloy in a molten salt environment of 75 wt% Na_2SO_4 and 25 wt% NaCl at 900 °C was studied, via oxidation kinetics analyses, scanning electron microscope observations and energy dispersive as well as diffraction analyses by X-ray. A multilayer corrosion oxide scale and dendritic morphology internal corrosion zone formed after hot corrosion, and inter-phase selective corrosion phenomena were also observed. Salt fluxing and oxidation-sulfidation processes were inferred to be the essential hot corrosion mechanisms of the alloy. Moreover, additions of Cr and Y proved to be beneficial to the hot corrosion resistance of the IC21 alloy, while the Mo content should be strictly controlled.

Keywords Hot corrosion · Ni_3Al-based alloy · Inter-phase selective corrosion · Molten salts

Introduction

The Ni_3Al-based alloys have become important candidates for hot components in turbine engines in recent years, owing to their high melting points (Tm $\geq$ 1,300 °C), low densities and excellent high-temperature performances [1]. Many Ni_3Al-based alloys with different alloying compositions have been developed and some of them have achieved even higher strength and higher creep rupture

W. Zhao (✉) · Y. Liu · S. Li · S. Gong
Key Laboratory of Aerospace Materials and Performance (Ministry of Education), School of Materials Science and Engineering, Beihang University, No. 37 Xueyuan Road, Beijing 100191, China
e-mail: wendyzhao56@buaa.edu.cn

strength than the traditional Ni-based superalloys above 1,050 °C [2, 3]. However, due to the development requirements of new generation engines with higher thrust-weight ratio, researches on improving the oxidation and corrosion resistances of Ni_3Al-based alloys in service environments are considered to be important. Although thermal barrier coatings are applied on the hot component surfaces, the hot corrosion behavior of the matrix alloy is still important at the locations like turbine blade cooling cavities. The oxidation and corrosion resistances of the Ni–Al alloys at high temperature could be improved via alloying design [4, 5].

In the present work, the hot corrosion behavior of a newly developed single-crystal Ni_3Al-based IC21 alloy in a molten salt environment of 75 wt% Na_2SO_4 and 25 wt% NaCl at 900 °C was studied. The hot corrosion kinetics, composition and microstructure of the hot corrosion oxide scale, and the hot corrosion mechanism of the alloy are discussed in this paper. The effects of the micro-alloying elements, such as Mo, Y, Cr and Re, on the high temperature behavior of the IC21 alloy were also investigated in order to improve the hot corrosion resistance of the alloy further.

Experimental Procedures

Materials and Specimens Preparation

The IC21 alloy with a cuboidal morphology microstructure composed of γ-Ni (Mo) solid solution phases and γ′-Ni_3Al strengthening phases was prepared via rapid directional solidification technology as well as subsequent solution and aging treatments. Based on the IC21 alloy composition, alloys with different alloying element contents listed in Table 1 were also prepared in order to study the effects of micro-alloying elements on the hot corrosion behavior of the alloy. Moreover, another typical Ni_3Al-based IC6 alloy (also see Table 1) was also prepared and tested in order to evaluate the hot corrosion resistance of the IC21 alloy.

The specimens for hot corrosion tests, with dimensions of $9 \times 9 \times 5$ mm^3, were ground and polished before tests. After hot corrosion tests, the alloy specimens were gold sprayed and nickel electroplated first for the purpose of scale protection. Then the cross-section specimens were produced by cold mosaic of the corroded alloy with condensable plastic to prevent the dissolution of the corrosion products.

Hot Corrosion Testing Methods

Hot corrosion tests in present study were implemented in a self-designed hot corrosion testing system (see Fig. 1). Salts with the composition of 75 wt% Na_2SO_4 and 25 wt% NaCl were contained by a quartz glass crucible and were placed in the atmosphere generation zone I of the system. Blowing laboratory air mixed with the molten salt atmosphere uniformly and the corroding atmosphere was taken into the reaction zone II by the driving of the concentration gradient and temperature gradient subsequently. The detailed construction and working mechanism of the system could be found in our previous work (see Ref. [6]). The hot corrosion tests of

Table 1 Compositions and microstructural parameters of the tested alloys in the present work

Alloy	Alloying elements	Compositional variation (vs. IC21)	Volume fraction of γ' (%)	Average sizes of γ' (nm)
IC21	Ni, Al, Mo, Re	–	71	440
IC21 + Y	Ni, Al, Mo, Re, Y	Addition of Y (0.1 wt%)	70	450
IC21 + Y + Cr	Ni, Al, Mo, Re, Y, Cr	Addition of Y (0.1 wt%) and Cr (2 wt%)	69	480
IC32	Ni, Al, Mo, Re, Ta	Addition of Ta (3 wt%), higher Re but lower Mo content	65	500
IC6	Ni, Al, Mo, B, C	Addition of B (<0.1 wt%) and C (<0.1 wt%), higher Mo content without Re	75	650

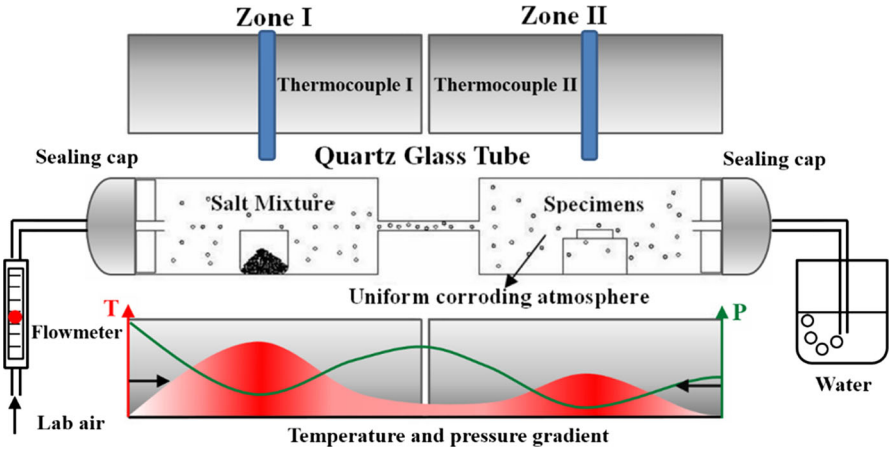

Fig. 1 Schematic diagram of the high temperature corrosion testing system

the alloys were carried out at 900 °C, while the molten salt atmosphere of 75 wt% Na_2SO_4 and 25 wt% NaCl was generated at 950 °C. The flow rate of the blowing air was about 100 ml/min. Different specimens were taken out of the furnace and air-cooled after different intervals of time. Three measurements of the weight gain per unit area of every specimen were recorded and calculated, and the average values were used to plot the kinetic curves. Microstructure observations and composition analyses were carried out by using a S4800 field-emission scanning electron microscope (SEM), X-ray dispersive spectrometer (EDS) and a D/max type X-ray diffractometer (XRD) with a Cu target. All the SEM images in the present work were collected in back-scattered electron (BSE) mode and the spatial resolution of EDS sampling volume was about 0.1 μm^3. As a comparison, hot corrosion test of

another representative Ni_3Al-based IC6 alloy was also carried out at 900 °C under the same test condition.

Results

Hot Corrosion Kinetics

The hot corrosion kinetics curve (weight gain curve) was plotted after the hot corrosion test of the IC21 alloy with molten salts of 75 wt% Na_2SO_4 and 25 wt% NaCl at 900 °C. As shown in Fig. 2a, the hot corrosion kinetics curve of the IC21 alloy has an obviously decreased slope after 22 h exposure. For comparison, the hot corrosion kinetics curve of the IC6 alloy was also plotted in Fig. 2b, which was almost obeyed the linear law with larger slope and had much greater weight gains than the IC21 alloy. This result indicates that the newly developed IC21 alloy has higher hot corrosion resistance than the IC6 alloy in the molten salts at 900 °C.

Composition and Microstructure of Hot Corrosion Oxide Scale

The hot corrosion products of the IC21 alloy were detected by XRD analyses after different exposure times. The results shown in Fig. 3 reveal that NiO and $NiAl_2O_4$ were the main products of the alloy in the molten salt environment. Moreover, low contents of $NiMoO_4$ and NiS were also detected when the exposure time was relatively short, which might form during the initial stage of the hot corrosion process or exist far below the oxide scale surface.

The typical cross-section morphology of the hot corrosion oxide scale on the IC21 alloy (see Fig. 4) shows that a multilayer corrosion oxide scale as well as a dendritic morphology internal corrosion zone formed after the hot corrosion in the molten salts. According to the cross-section EDS analysis results of the hot corrosion oxide scale (see Table 2; Fig. 5) and the previous XRD results, the oxide layer A of the alloy was a columnar zone with single oxide NiO, while the oxide

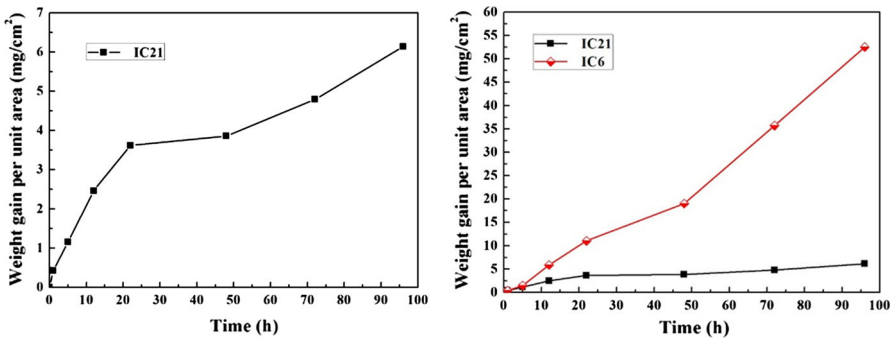

Fig. 2 Hot corrosion kinetics curves of the IC21 alloy (**a** and **b**) and the IC6 alloy (**b**) at 900 °C with molten salts

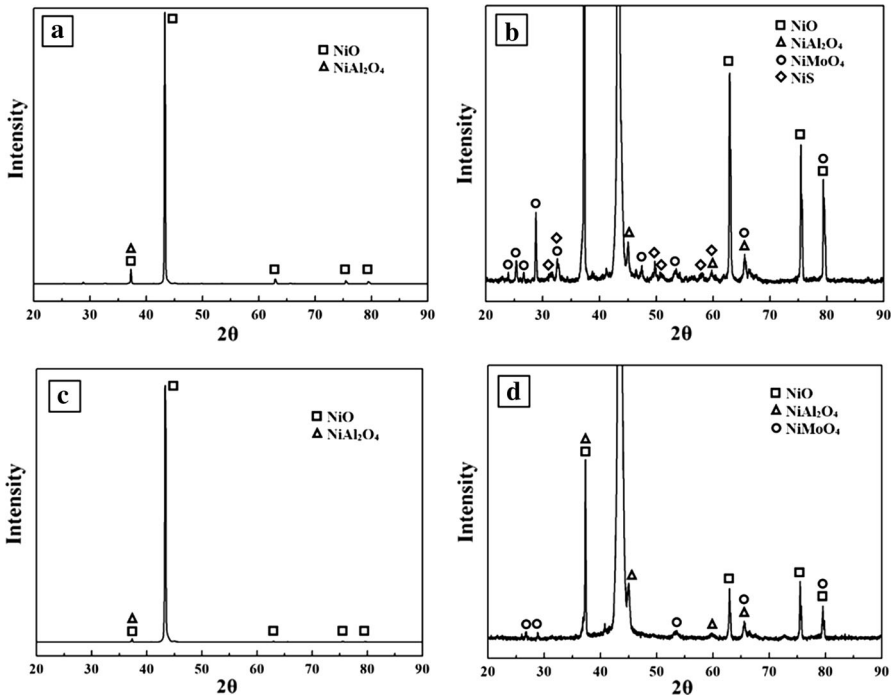

Fig. 3 XRD analysis results of the IC21 alloy after hot corrosion with molten salts at 900 °C: **a**, **b** for 12 h; **c**, **d** for 48 h; **a**, **c** full spectra; **b**, **d** magnification of low-intensity peaks

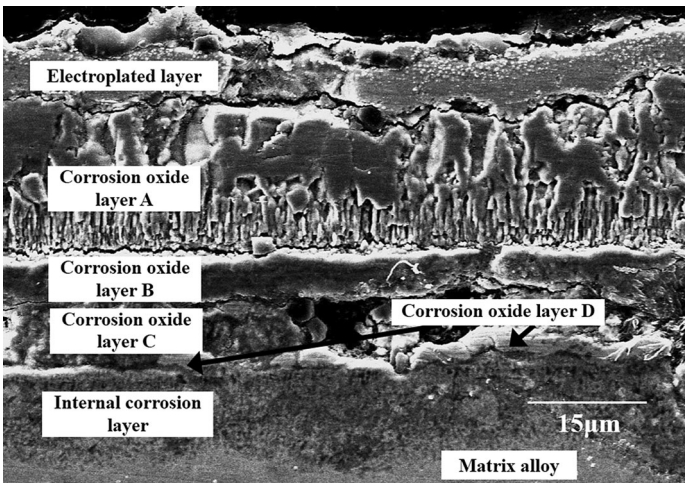

Fig. 4 Cross-section morphology (BSE image) of the IC21 alloy specimen after hot corrosion at 900 °C with molten salts for 48 h

Table 2 EDS results of different layer structures in the hot corrosion oxide scale of the IC21 alloy

Atomic percent	Outer oxide layer A	Outer oxide layer B	Outer oxide layer C	Outer oxide layer D	Dark parts in internal oxidation zone	Grey parts in internal oxidation zone
Ni	59.1	27.2	15.7	16.7	50.9	79.5
Al	–	31.4	16.8	19.8	18.9	13.3
O	40.9	41.4	50.2	26.8	24.1	–
S	–	–	17.3	36.7	1.0	–
Mo	–	–	–	–	5.0	7.2

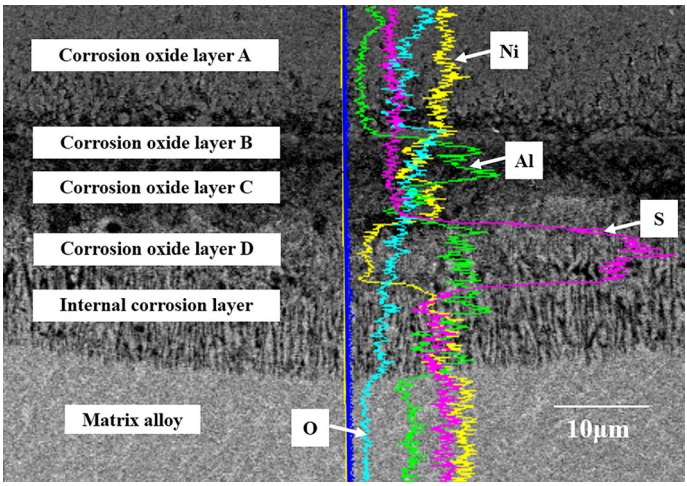

Fig. 5 EDS line scan results of the hot corrosion oxide scale after 48 h exposure at 900 °C

layers B, C and D have higher contents of Al and $NiAl_2O_4$ was considered to be the main oxide product of these layers. It is noteworthy that obvious higher contents of S with depletion of Ni were discovered in the oxide layers C and D, which indicates that sulfidation corrosion products NiS_x and AlS_x probably existed in these locations. In addition, the dark grey parts of the dendritic morphology internal corrosion zone in the BSE image were proved to be internal corrosion products with higher content of O and S while the light grey parts were the residual matrix alloy with a similar composition to γ-Ni (Mo). Although the hot corrosion oxide scale of the alloy was loose and porous, the interface between the internal corrosion zone and the matrix alloy was relatively straight.

Inter-phase Selective Corrosion of the Cuboidal Microstructure

As demonstrated in Fig. 6, the original microstructure of the Ni_3Al-based IC21 alloy was composed with cuboidal γ′-Ni_3Al phases and reticular γ-Ni (Mo) phases. In

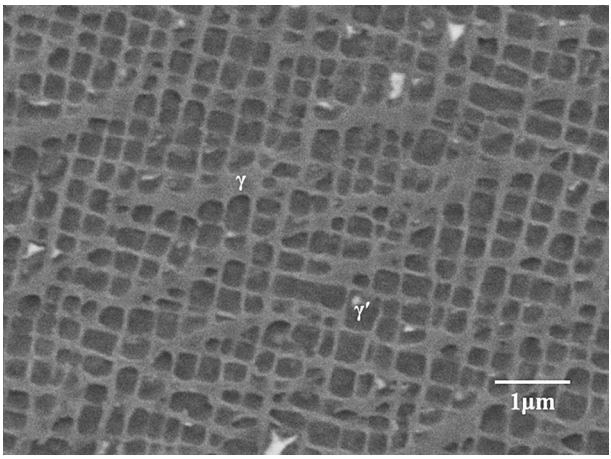

Fig. 6 Cuboidal morphology (BSE image) of the original microstructure in the IC21 alloy

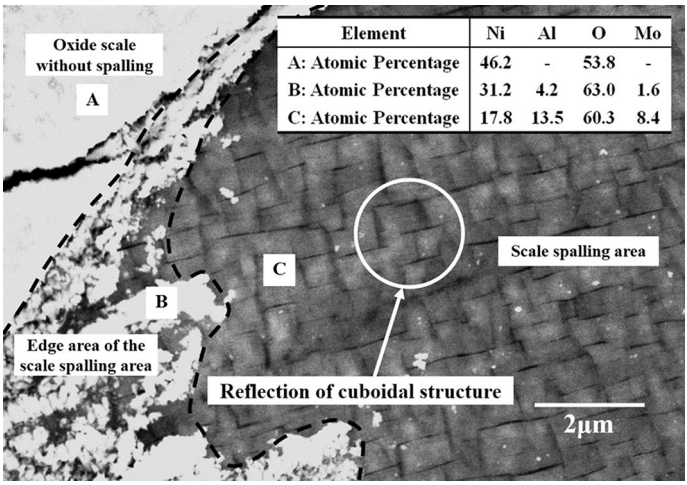

Fig. 7 Composition and microstructure morphology of the scale spalling nearby area on the IC21 alloy surface after hot corrosion at 900 °C with molten salts for 5 min

order to study the relationship between the hot corrosion behavior of the alloy and its microstructure, hot corrosion tests with ultra-short exposure times but increased molten salt atmosphere concentration were conducted by decreasing the blowing air flow in the hot corrosion testing system. Through this kind of accelerated hot corrosion test, valuable information on long-time corrosion behavior could be obtained with very short experimental exposure time. Both surface and cross-section morphologies of the corrosion oxide scale were observed via SEM (see Figs. 7, 8).

After exposure in the corroding environment for 5 min, different thicknesses of corrosion products deposited on different areas of the alloy surface (see Fig. 7). Especially at the local scale spalling area in Fig. 7 which was the result of the high

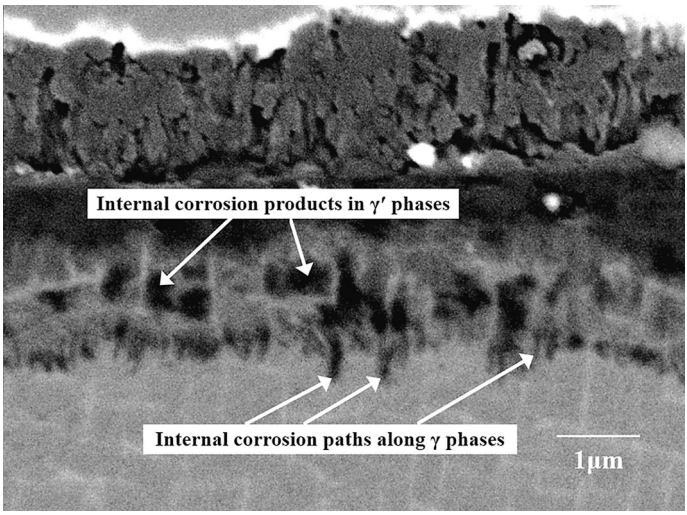

Fig. 8 Cross-section morphology (BSE image) of the internal corrosion layer in the IC21 alloy after hot corrosion at 900 °C with molten salts for 10 min

cooling rate during air cooling, the surface morphology of the corrosion oxide scale are considered to reflect the original cuboidal microstructure of the alloy via comparing their shapes and microscopic dimensions. More oxides deposited mainly at the cuboidal γ' phases and made protuberant morphologies consequently. This phenomenon is considered to result from the corrosion rate differences between the two phases, which is called inter-phase selective corrosion [6]. The EDS analysis results shown in Fig. 7 demonstrate that these oxides (location C) had higher contents of Al and Mo than the edge area of the scale spalling area (location B), while the outmost surface of the scale (location A) was only NiO. These results indicate that the corrosion reactions involving Al dominated the initial stage of the hot corrosion process, so more corrosion products were generated on the γ' phases which had higher content of Al. Moreover, Mo might also participate in the initial hot corrosion reaction. However, few corrosion products of Mo with molten salts could be detected because of their high volatility and the higher Mo content found in the scale spalling area might come from the matrix alloy below owing to the filmy scale. The outward diffusion and oxidation of Ni would happen soon as the hot corrosion proceeding, and a large amount of NiO produced. Due to the small difference of Ni content between γ and γ' phases, the cuboidal morphology of the oxide scale surface disappeared and a single outmost NiO layer formed eventually.

Similar cuboidal morphology was also discovered in the cross-section image of the internal corrosion zone after hot corrosion for 10 min in the increased concentration of molten salt atmosphere (see Fig. 8). The cuboidal internal oxides had nearly the same sizes and distribution as the γ' phases in the original alloy, while the residual matrix alloy had also similar composition to γ phase. However, this cuboidal morphology changed into dendritic morphology obviously near the interface between the internal corrosion zone and the matrix alloy, and some

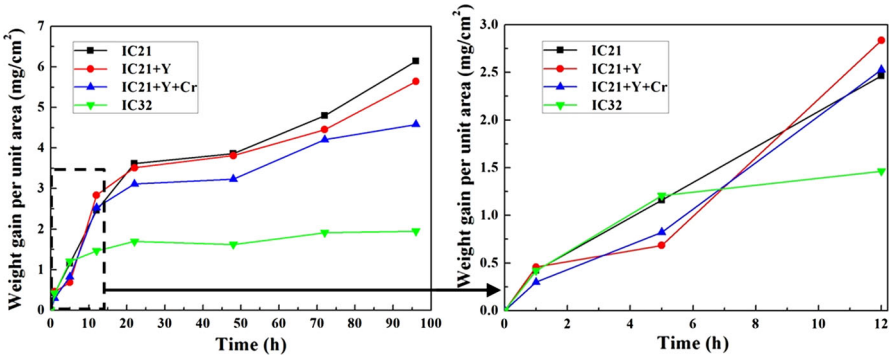

Fig. 9 Hot corrosion kinetics curves of the Ni_3Al-based alloys with different compositions at 900 °C with molten salts

internal corrosion paths along the γ phases penetrated into the matrix alloy showed up. These phenomena were also considered to result from the inter-phase selective corrosion of the alloy which will be discussed in detail later.

The Effects of Micro-alloying Elements on the Hot Corrosion Resistance

In order to improve the hot corrosion resistance of the IC21 alloy in molten salt environment and to optimize the alloy system, the effects of micro-alloying elements on hot corrosion resistance were studied via the hot corrosion testing of the alloys with different compositions based on the IC21 alloy system at 900 °C with the molten salts. The possible effects of the original microstructure on hot corrosion behavior had been eliminated through proper heat treatments before hot corrosion tests, by which similar sizes and volume percentages of γ′ phases had been achieved in the alloys with different addition of micro-alloying elements (see Table 1). Figure 9 demonstrates the hot corrosion kinetics curves of the micro-alloyed alloys as compared with the original IC21 alloy. It is clear that the IC32 alloy had the best hot corrosion resistance, while the alloys with addition of Y and Y + Cr had similar shapes of the kinetics curves to the original IC21 alloy but obvious lower weight gains per unit area after 22 h exposure in the molten salt environment.

The hot corrosion products of the Ni_3Al-based alloys with different compositions were also detected via XRD analyses. The results shown in Fig. 10 reveal that the hot corrosion products in the micro-alloyed alloys were the same as the ones in the original IC21 alloy and no new product containing Y, Cr, or Ta was discovered except the relative content of $NiAl_2O_4$ was increased after micro-alloying with Y and Y + Cr.

The cross-section morphology observations and composition analyses of the hot corrosion oxide scales in the Ni_3Al-based alloys with different compositions were conducted as well (see Fig. 11). The results demonstrate that similar multilayer corrosion oxide scales and dendritic morphology internal corrosion zones also formed on the alloy surfaces. However, the thickness of the internal corrosion zones in all micro-alloyed alloys decreased, while the thickness of the corrosion oxide scale was also decreased obviously in the IC32 alloy. Moreover, much fewer S

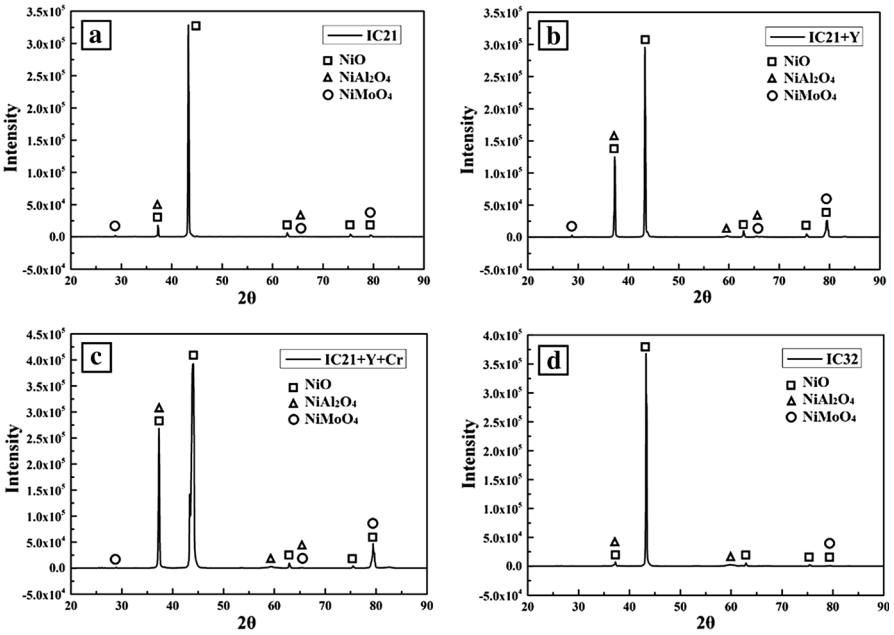

Fig. 10 XRD analysis results of the Ni_3Al-based alloys with different compositions after hot corrosion with molten salts at 900 °C for 12 h: **a** IC21; **b** IC21 + Y; **c** IC21 + Y + Cr; **d** IC32

contents (1.77 at.%) were detected below NiO layer in the IC21 + Y alloy and S was even absent in the IC21 + Y + Cr and IC32 alloys. Especially, only NiO and $NiAl_2O_4$ oxide layers formed on the IC32 alloy surface after hot corrosion in molten salts. Corresponding to the segregation of Al in the oxide layers below the NiO layer, depletions of Ni were also appeared in the IC21 + Y and IC21 + Y + Cr alloys which suggest that the hot corrosion micro-processes might not change in these micro-alloyed alloys. Low content of Cr (about 2–3 at.%) was also detected in the oxide scale of the IC21 + Y + Cr alloy which indicates that oxides of Cr formed during hot corrosion of the alloy. However, these oxides of Cr had not been detected by XRD due to the low alloying content of Cr as well as the larger depth of their locations from the surface.

The experimental results mentioned above show that the effects of Y and Cr on the hot corrosion behavior of the IC21 alloys were relatively small but they still improved the hot resistance of the alloy at some extent. On the other hand, the IC32 alloy had the best hot corrosion resistance in the molten salt environment at 900 °C compared to the original IC21 alloy and other micro-alloyed alloys.

Discussion

After hot corrosion in a molten salt environment at 900 °C, multilayer corrosion oxide scales and dendritic morphology internal corrosion zone were found on the

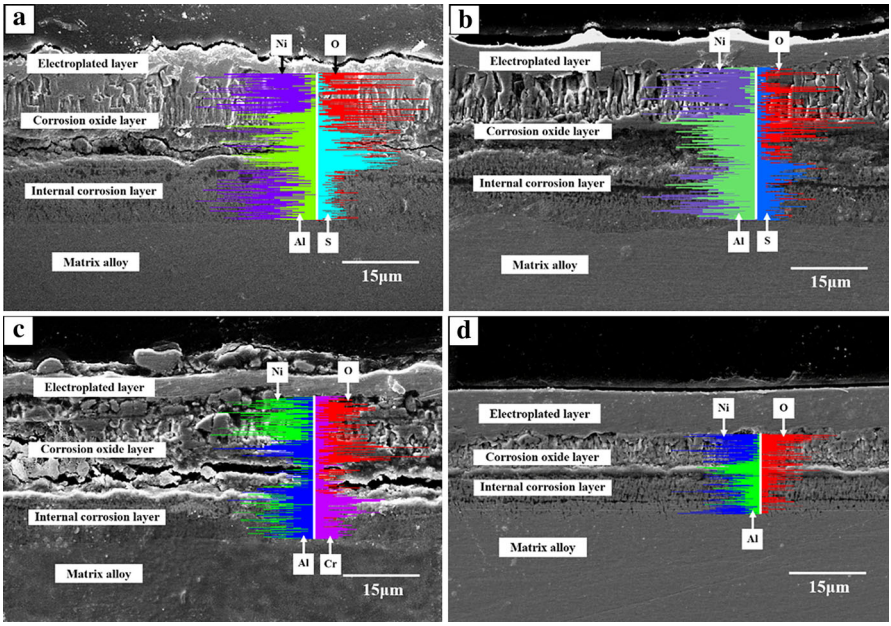

Fig. 11 Cross-section morphologies (BSE images) and EDS line scan results of the oxide scales on the Ni_3Al-based alloys with different compositions after hot corrosion at 900 °C with molten salts for 12 h: **a** IC21; **b** IC21 + Y; **c** IC21 + Y + Cr; **d** IC32

surface of the IC21 alloy, accompanied with the segregation of sulfides and the depletion of Ni. All these hot corrosion behavior characteristics proved that the IC21 alloy suffered a Type I hot corrosion [i.e. high temperature hot corrosion (HTHC)] process at 900 °C [7].

Many models such as the salt fluxing model, electrochemical model and sulfidation-oxidation model are considered to be the main hot corrosion mechanisms in Ni-based superalloys which have similar γ'-Ni_3Al + γ-Ni(Mo) microstructures with the Ni_3Al-based alloys. According to the oxide solubility measurements in molten Na_2SO_4 by Rapp et al., [8] it is argued that Al_2O_3 is prone to dissolution in molten salts via the combination with O^{2-} to form AlO^{2-} anions, which is called the basic fluxing mechanism. On the other hand, a large number of experiments have proved that the hot corrosion mechanism of Ni in molten salts is a coupling mechanism with sulfidation and basic fluxing, although NiO is a much more basic oxide [8]. The alloying element Mo also has important influences on the hot corrosion behavior of the alloy. The high volatility of the oxides of Mo and the self-sustaining acid fluxing of these oxides in molten salts will increase the local acidity of the salt film and destroy the protective oxide scale [8]. As a result, the alloying content of Mo must to be controlled strictly in alloy design. Although the Ni_3Al-based IC21 alloy has higher content of Al and higher volume percentage of γ' phase than the ones in the traditional Ni-based superalloys, the corrosion reactions associated with Ni still dominated the hot corrosion process of the IC21 alloy and no

protective oxide scale of Al_2O_3 formed. Consequently, salt fluxing and oxidation-sulfidation processes are considered to be the essential hot corrosion mechanisms of the IC21 alloy, and both basic fluxing and acid fluxing might be involved owing to the relatively high content of Mo in the alloy.

Based on the experimental results obtained in the present work, the hot corrosion microscopic process of the IC21 alloy at 900 °C is considered as follows. In the initial stage, element Al is oxidized preferentially due to its more negative oxidation Gibbs free energy and thicker alumina forms on the γ' phase surface which has higher content of Al. As a result, protuberant morphologies show up on the cubic γ' phase surfaces which is called the inter-phase selective corrosion phenomenon. At the same time, more acid environment is produced via the reactions of the Mo oxides with the molten salts, and the acid fluxing process of Al_2O_3 destroys the continuity of the scale and makes it non-protective. Subsequently, element Ni participates in the oxidation reactions soon which has lower activity but higher diffusion rate than Al. NiO oxide layer forms through the outward diffusion of Ni atoms and the inter-phase selective corrosion phenomenon disappears due to the small content difference of Ni between γ and γ' phases. Besides the competition between the oxidation of Ni and Al, complex oxides $NiAl_2O_4$ are also produced via the reaction of NiO with Al_2O_3. As the continuous oxidation of Ni proceeds, the partial pressure of oxygen near the alloy surface reduces and the partial pressure of sulfur increases accordingly. Owing to the non-protective oxide scale, the partial pressure of sulfur at the matrix alloy surface will be higher than the one at the interface between molten salts and gas generally [9]. As a result, NiS_x forms due to the higher sensitivity of Ni with sulfur, and these sulfides make the basic fluxing of NiO happen by changing the acid–base property of the molten salt film. The sulfides are unstable and some of them will change into NiO or complex oxides $NiAl_2O_4$ with the increasing partial pressure of oxygen subsequently. In this stage, Ni atoms are consumed greatly via the outward diffusion of Ni and the inward diffusions of O and S atoms, the interface between the oxide scale and the matrix alloy migrates inward and depletion of Ni shows up as the result. Finally, internal corrosion occurs as the corrosion reactions carrying through. The invasions of O and S into the interface between the oxide scale and the matrix alloy lead to the "diffusionless" or "in situ" internal corrosion of the matrix alloy [10, 11]. Based on the fact that the attack of aluminum is thermodynamically favored, internal oxides with the similar shape and distribution to γ' phases form firstly, which is also considered to be the consequence of the inter-phase selective corrosion. However, owing to the higher sensitivity of Ni with sulfur and the higher growth rates of NiS_x, γ phases with higher Ni content become the preferential internal corrosion locations instead of γ' phases soon. As a result, internal corrosion paths along γ phases show up below the initial internal corrosion zone. As the internal corrosion reactions proceeding, the cuboidal morphology of the internal corrosion zone changes into dendritic morphology finally, via the rapid internal corrosion of γ phases.

Several kinds of micro-alloying elements were added into the IC21 alloy in order to improve the hot corrosion resistance of the alloy in the molten salt environment. The element Y has been considered to improve the scale adhesion

property and to strengthen the oxide scale of the Ni_3Al-based IC6 alloy through retarding the sulfur transport and segregating itself at the oxide grain boundaries respectively [12]. Similarly, the hot corrosion resistance of the IC21 + Y alloy in molten salts has also been improved with reduced weight gains, better scale adhesion and less sulfur segregation in the oxide scale. However, the elevation degree is still limited due to the small additive amount of Y in the alloy. The element Cr is also beneficial to the hot corrosion resistance of Ni–Al alloys which can promote the formation of protective α-Al_2O_3 [4]. The acid oxide Cr_2O_3 can produce ions via basic fluxing process and protective Cr_2O_3 can be re-produced by the reduction reaction at boundaries or crack locations in the oxide scale, which can impede the sulfidation of Ni [13]. The formation of Cr_2O_3 and no sulfur segregation were found in the hot corrosion process of the IC21 + Y + Cr alloy as well, which suggests that the addition of Cr has hindered the internal invasion of S and O effectively. On the other hand, because of the low content of Re and Ta in the IC32 alloy as well as no corrosion products of these micro-alloying elements being detected, the obvious improved hot corrosion resistance of the alloy is considered to result from the Mo content reduction. As mentioned above, the element Mo has severe negative influences on the oxidation and corrosion behavior of Ni-based superalloys at high temperature. Comparing the hot corrosion behaviors of the IC32, IC21 and IC6 alloys in which the Mo content increases in sequence (see Table 1), the EDS composition analysis results of corrosion oxide scales in these alloys reveal that lower Mo content can retard the acid fluxing process of Al_2O_3 oxides and enhance the oxide scale resistance from sulfur invasion. In other words, the Mo content of the Ni_3Al-based alloy should be selected carefully based on the comprehensive considerations of mechanical properties and hot corrosion resistance.

Conclusions

The newly developed single-crystal Ni_3Al-based IC21 alloy had higher hot corrosion resistance than the IC6 alloy in a molten salt environment of 75 wt% Na_2SO_4 and 25 wt% NaCl at 900 °C. NiO, $NiAl_2O_4$ and NiS were the main corrosion products of the IC21 alloy. Multilayer corrosion oxide scales and dendritic morphology internal corrosion zone formed after hot corrosion, and the segregation of S with depletion of Ni was also discovered in the complex oxide-sulfide layer. Salt fluxing and oxidation-sulfidation processes are considered to be the essential hot corrosion mechanisms of the IC21 alloy, and both basic fluxing and acid fluxing were involved due to the higher content of Mo in the alloy. Inter-phase selective corrosion phenomena were also observed during the hot corrosion process of the IC21 alloy, which had a close relation to the morphologic features and the compositions of the two phases in the alloy. Based on the comprehensive considerations of mechanical properties and hot corrosion resistance, proper additions of Y and Cr can improved the hot corrosion resistance of the IC21 alloy while the Mo content should be controlled strictly.

References

1. R. F. Zhou, Y. F. Han and S. S. Li, *High Temperature Structure Materials*, (National Defense Industry Press, Beijing, 2006).
2. Y. G. Zhang, Y. F. Han, G. L. Chen, J. T. Guo, X. J. Wan and D. Feng, *Structural Intermetallics*, (National Defense Industry Press, Beijing, 2001).
3. Y. X. Lu, W. X. Chen and R. Eadie, *Intermetallics* **12**, 2004 (1299).
4. J. Klöwer, U. Brill and U. Heubner, *Intermetallics* **7**, 1999 (1183).
5. P. Y. Hou, T. Izumi and B. Gleeson, *Oxidation of Metals* **72**, 2009 (109).
6. W. Zhao, B. Xu, Y. Ma and S. Gong, *Progress in Natural Science: Materials International* **21**, 2011 (322).
7. N. Eliaz, G. Shemesh and R. M. Latanision, *Engineering Failure Analysis* **9**, 2002 (31).
8. R. A. Rapp, *Corrosion Science* **44**, 2002 (209).
9. W. H. Lee and R. Y. Lin, *Material Chemistry and Physics* **77**, 2002 (86).
10. F. Gesmundo, F. Viani and Y. Niu, *Oxidation of Metals* **42**, 1994 (409).
11. F. Gesmundo, Y. Niu and F. Viani, *Oxidation of Metals* **43**, 1995 (379).
12. Y. F. Han and C. B. Xiao, *Intermetallics* **8**, 2000 (687).
13. N. Otsuka and R. A. Rapp, *Journal of the Electrochemical Society* **137**, 1990 (53).